Electron correlation in two-photon double ionization of helium from attosecond to XFEL pulses

J Feist[1], **R Pazourek**[1], **S Nagele**[1], **E Persson**[1], **B I Schneider**[2,3], **L A Collins**[4] **and J Burgdörfer**[1]

[1] Institute for Theoretical Physics, Vienna University of Technology, 1040 Vienna, Austria
[2] Physics Division, National Science Foundation, Arlington, Virginia 22230, USA
[3] Electron and Atomic Physics Division, National Institute of Standards and Technology, Gaithersburg, Maryland 20899, USA
[4] Theoretical Division, Los Alamos National Laboratory, Los Alamos, New Mexico 87545, USA

E-mail: johannes.feist@tuwien.ac.at

Abstract
We investigate the role of electron correlation in the two-photon double ionization of helium for ultrashort pulses in the extreme ultraviolet (XUV) regime with durations ranging from a hundred attoseconds to a few femtoseconds. We perform time-dependent *ab initio* calculations for pulses with mean frequencies in the so-called 'sequential' regime ($\hbar\omega > 54.4$ eV). Electron correlation induced by the time correlation between emission events manifests itself in the angular distribution of the ejected electrons, which strongly depends on the energy sharing between them. We show that for ultrashort pulses two-photon double ionization probabilities scale non-uniformly with pulse duration depending on the energy sharing between the electrons. Most interestingly we find evidence for an interference between direct ('nonsequential') and indirect ('sequential') double photoionization with intermediate shake-up states, the strength of which is controlled by the pulse duration. This observation may provide a route towards measuring the pulse duration of x-ray free-electron laser (XFEL) pulses.

(Some figures in this article are in colour only in the electronic version)

1. Introduction

The role of electron correlation is of central interest in our understanding of atoms, molecules and solids. The recent progress in the development of ultrashort and intense light sources [1–10] provides unprecedented opportunities to study the effects of correlation not only in stationary states, but also in transient states (i.e., resonances), and even to actively induce dynamical correlations [11].

The helium atom is the simplest atomic system where electron–electron interactions can be studied, with its double ionization being the prototype reaction for a three-body Coulomb breakup. While computationally challenging, the full dynamics of the helium atom can still be accurately simulated in *ab initio* calculations [12]. With the advent of intense XUV pulses, the focus has shifted from single-photon double ionization [13–17] and intense-IR laser ionization by rescattering ([18–20] and references therein) to multiphoton ionization. Two-photon double ionization (TPDI) has recently received considerable attention, both in the so-called 'nonsequential' or 'direct' regime (39.5 eV $< \hbar\omega <$ 54.4 eV), where the electrons necessarily have to share energy via electron–electron interaction to achieve double ionization [21–34], and in the 'sequential' regime ($\hbar\omega > 54.4$ eV), where electron–electron interaction is not *a priori* necessary [11, 35–40].

In a previous paper [11], we investigated the role of energy and angular correlations in the shortest pulses available today, where the distinction between 'sequential' and 'nonsequential' becomes obsolete. In this contribution, we explore the

dependence of TPDI on the pulse duration T_p ranging from ~100 attoseconds (the duration of the shortest pulses produced by high-harmonic generation [3]) to a few femtoseconds (the expected duration of XFEL pulse 'bursts'). T_p can be used as a control knob to change from a 'direct' to an 'indirect' process. In section 3, we discuss the behaviour of the one-electron ionization rate $P^{DI}(E)/T_p$, which displays non-uniform scaling with T_p. In section 4, we investigate the angular correlations, with a focus on longer pulses, which reveal the detailed dynamics of the TPDI process. In section 5, we show that for energies above the threshold associated with shake-up ionization of the He atom, interferences between sequential and nonsequential contributions can be observed, the strength of which can be varied by changing the pulse duration. One consequence is that from the size and shape of these Fano-like resonances, the pulse duration of XUV pulses might be deduced. All this information is encoded in the final joint momentum distribution $P^{DI}(\mathbf{k}_1, \mathbf{k}_2) \equiv P^{DI}(E_1, E_2, \Omega_1, \Omega_2)$, which is experimentally accessible in kinematically complete cold-target recoil-ion-momentum spectroscopy (COLTRIMS) measurements [41]. In this contribution, we focus on integrated quantities, which are more readily accessible because of better statistics. Unless otherwise stated, atomic units are used.

2. Method

Our theoretical approach (described in more detail in [30]) is based on a direct solution of the time-dependent Schrödinger equation by the time-dependent close-coupling (TDCC) scheme [22, 24, 35, 42]. The time-dependent Schrödinger equation is solved in its full dimensionality including all inter-particle interactions. The laser field is linearly polarized and treated in dipole approximation. The interaction operator is implemented in both length and velocity gauge, such that gauge independence can be explicitly checked. In the TDCC scheme the angular part of the wavefunction is expanded in coupled spherical harmonics. For the discretization of the radial functions, we employ a finite element discrete variable representation (FEDVR) [43–46]. A local DVR basis within each finite element leads to a diagonal representation of all potential energy matrices. The sparse structure of the kinetic energy matrices enables efficient parallelization, giving us the possibility of employing pulses with comparably long durations (up to a few femtoseconds) in our simulations. For the temporal propagation of the wavefunction, we employ the short iterative Lanczos method [47–49] with adaptive time-step control.

Dynamical information is obtained by projecting the wave packet onto products of Coulomb continuum states. As these independent-particle Coulomb wavefunctions are not solutions of the full Hamiltonian, projection errors are, in principle, inevitable. However, since we are able to propagate the wavepacket for long times after the conclusion of the pulse, errors in the asymptotic momentum distribution can be reduced to the 1% level by delaying the time of projection until the two electrons are sufficiently far apart from each other [30].

Most of the results presented were obtained at a mean photon energy of $\hbar\omega = 70\,\mathrm{eV}$, which would correspond to the sequential regime for long pulses. We choose the vector potential to be of the form

$$\mathbf{A}(t) = \hat{\mathbf{z}}A_0 \sin^2(\pi t/(2T_p)) \sin(\omega t) \tag{1}$$

for $0 < t < 2T_p$. The duration T_p corresponds to the FWHM of the sine-squared envelope function. The peak intensity was chosen as $I_0 = 10^{12}\,\mathrm{W\,cm^{-2}}$ to ensure that ground state depletion and three-or-more-photon effects are negligible. In order to reach convergence of the angular distribution, single electron angular momenta up to values of $l_{1,\mathrm{max}} = l_{2,\mathrm{max}} = 10$ were used. The highest total angular momentum included in the time propagation was $L_{\mathrm{max}} = 3$. For extracting the final probability distributions, only the two-photon channels $L = 0$ and $L = 2$ were taken into account. The radial grid was composed of FEDVR elements of 4 au with order 11, with an extension up to $r_{\mathrm{max}} = 800\,\mathrm{au}$ for the longest pulses. All presented quantities were tested for numerical convergence and gauge independence.

3. Pulse length dependence of TPDI

The nature of the two-photon double ionization process depends strongly on the photon energy. In order to doubly ionize the helium atom (ground state energy $E_0 \approx -79\,\mathrm{eV}$), each photon must have an energy of at least $\hbar\omega = -E_0/2 \approx 39.5\,\mathrm{eV}$. For $39.5\,\mathrm{eV} < \hbar\omega < 54.4\,\mathrm{eV}$, a single photon does not provide sufficient energy to ionize the He$^+$ ion. Thus, TPDI can only occur if the two electrons exchange energy during the ionization process. In a temporal picture, this implies that the 'first', already ejected, electron still has to be close to the nucleus when the second photon is absorbed, i.e., both photons have to be absorbed quasi-simultaneously (or nonsequentially). For photon energies larger than the ground state energy of the He$^+$ ion ($\hbar\omega > 54.4\,\mathrm{eV}$), an independent-particle picture is applicable for long pulses: each electron absorbs one photon and electron–electron interaction is *a priori* not required for double ionization to occur. The first electron is released from the He atom with an energy of $E_1 = \hbar\omega - I_1$, while the second electron is released from the He$^+$ ion with an energy of $E_2 = \hbar\omega - I_2$. Here, $I_1 \approx 24.6\,\mathrm{eV}$ ($I_2 \approx 54.4\,\mathrm{eV}$) is the first (second) ionization potential of helium. For shake-up satellites the partitioning of ionization potentials is different ($I_2' = I_2/n^2$), and so are the peak positions $E_{1,2}'$, but the overall picture of sequential and independent photoionization events remains unchanged.

For ultrashort pulses of a few hundred attoseconds, the notion of sequentiality loses its meaning. The breakdown of the independent-particle picture and strong coupling between the outgoing electrons is in that case not imposed by the necessity of energy sharing but is enforced by the ultrashort time between the two photoemission events occurring within T_p. Electron–electron interaction therefore plays a decisive role in the correlated final momentum distribution. In particular, the electrons are preferably emitted in a back-to-back configuration at approximately equal energy sharing, corresponding to a Wannier ridge configuration [11].
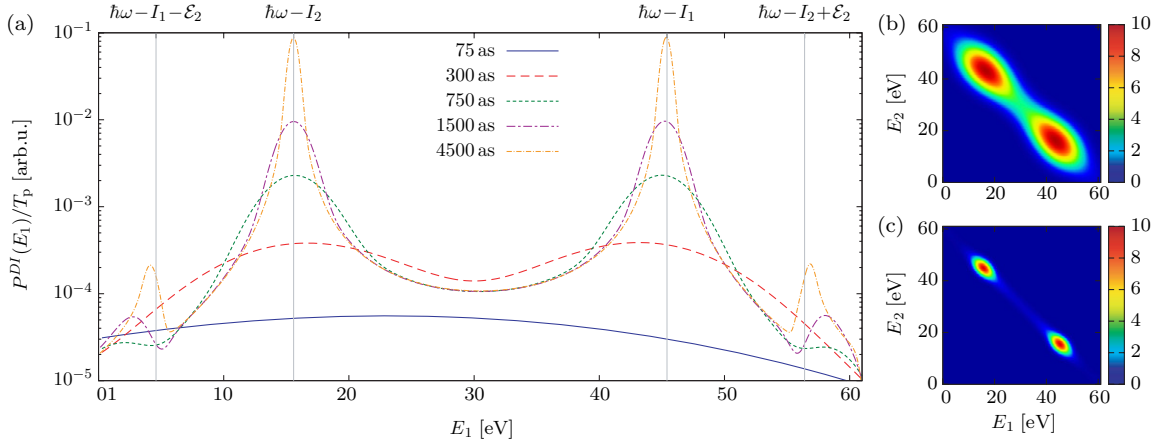
Figure 1. (a) Double ionization (DI) rate $P^{DI}(E)/T_p$ (i.e., DI probability divided by the pulse duration) for TPDI by an XUV pulse at $\hbar\omega = 70$ eV with different pulse durations T_p. For sufficient pulse duration, the DI rate converges to a stable value except near the peaks of the sequential process. (b) and (c) show the two-electron energy spectrum $P^{DI}(E_1, E_2)$ for (b) $T_p = 300$ as and (c) $T_p = 750$ as.

A key indicator for sequential TPDI is that for sufficiently low intensities (when ground state depletion is negligible), the total yield scales with $P_{seq}^{DI} \propto \int_{-\infty}^{\infty} \int_{t}^{\infty} I(t)I(t')\,dt'\,dt \propto T_p^2$, where T_p is the duration of the laser pulse [30, 37]. This is an immediate consequence of two independent subsequent emission processes, the probability for each of which increases linearly with T_p, such that $P_{seq}^{DI} \sim (P^I)^2 \propto T_p^2$. Equivalently, for each of the two processes a well-defined transition rate $W = \lim_{T_p \to \infty} P^I/T_p$ exists. This implies that the total rate P_{seq}^{DI}/T_p of the two-step process grows linearly with T_p in the limit of long pulses. By contrast, the nonsequential or direct double ionization probability P_{nonseq}^{DI} scales linearly with T_p and a converged transition rate exists in the limit $W = \lim_{T_p \to \infty} P_{nonseq}^{DI}/T_p$.

For ultrashort pulses, the scaling of the ionization yield with T_p varies between T_p and T_p^2, highlighting the non-uniform convergence over different regions of the electron emission spectrum and the breakdown of the distinction between direct and indirect processes. Figure 1(a) shows the energy differential electron emission probability (projection of the joint energy distribution figure 1(b), (c), onto the E_1 or E_2 axis) for different pulse durations, divided by T_p, $dW/dE = P^{DI}(E)/T_p$. This quantity converges to a duration-independent cross section value (apart from constant factors) except in the regions near $E = \hbar\omega - I_1$ and $E = \hbar\omega - I_2$, i.e., those values of the energy where the sequential process is allowed [39]. The peak areas grow linearly with T_p indicative of an overall quadratic scaling characteristic for the sequential process (cf figure 2(a)). If one divides the yield contained in the peak areas by T_p^2, the result is just proportional to the product of the single ionization cross sections for one-photon absorption from the He ground state and one-photon absorption from the He$^+$ ground state.

The region within which the linear scaling prevails is determined by the pulse duration for two different reasons:

(i) Due to Fourier broadening, the photon energy is not well defined for a finite pulse, limiting the energy resolution. Thus, if the broadened sequential peak overlaps with the

final energy of interest, the long-pulse limit $P^{DI}(E) \propto T_p$ cannot be observed.

(ii) There is an intrinsic maximum time delay between ionization events that can lead to a specific combination of final energies of the ejected electrons. When the second electron is ionized at a time when the first electron is already far from the nucleus, the electrons cannot exchange a sufficient amount of energy. For each final state, there is a maximum delay $t_c^{(ii)}$ between ionization events that can lead to that specific energy sharing. This implies that the pulse has to be considerably longer than this maximal delay in order to resolve all contributions to a specific final state.

In order to estimate the size of effect (ii), we employ a simple classical model: the first electron is emitted with energy $E_{SI} = \hbar\omega - I_1$. In order to reach a specific final state with energies (E_1, E_2), the liberated electron has to gain or lose the energy $\Delta E = \min(|E_{SI} - E_1|, |E_{SI} - E_2|)$ by interacting with the second electron. Therefore, the first electron can be at most a distance $r_{SI}(t_c^{(ii)}) = 1/\Delta E$ from the core at the moment of the second photon absorption. This leads to a critical time

$$t_c^{(ii)} = \frac{2\sqrt{\alpha(\alpha+1)} - \ln(2\alpha + 2\sqrt{\alpha(\alpha+1)} + 1)}{(2E_{SI})^{3/2}}, \quad (2)$$

with $\alpha = E_{SI}/\Delta E$.

Likewise, the spectral width of the pulse gives a corresponding time $t_c^{(i)} = 1/\Delta E$. Linear scaling should be observed for pulse durations T_c much longer than $t_c^{(i,ii)}$. Setting $T_c^{(i,ii)} \approx 10 t_c^{(i,ii)}$ leads to good agreement with the full numerical simulation (figure 2(b)). Moreover, both criteria give similar results thereby precluding a clear distinction between them. Figure 2(b) displays the estimates $T_c^{(i,ii)}$ and the fraction of double ionization probability that scales linear with T_p as a function of emission energy and pulse duration

$$P_{rel}^{DI}(E, T_p) = \frac{P^{DI}(E, T_p)}{P^{DI}(E, T_{max})} \frac{T_{max}}{T_p}, \quad (3)$$

where $T_{max} = 4.5$ fs is the longest pulse we used. P_{rel}^{DI} takes on the value one when the double ionization probability at

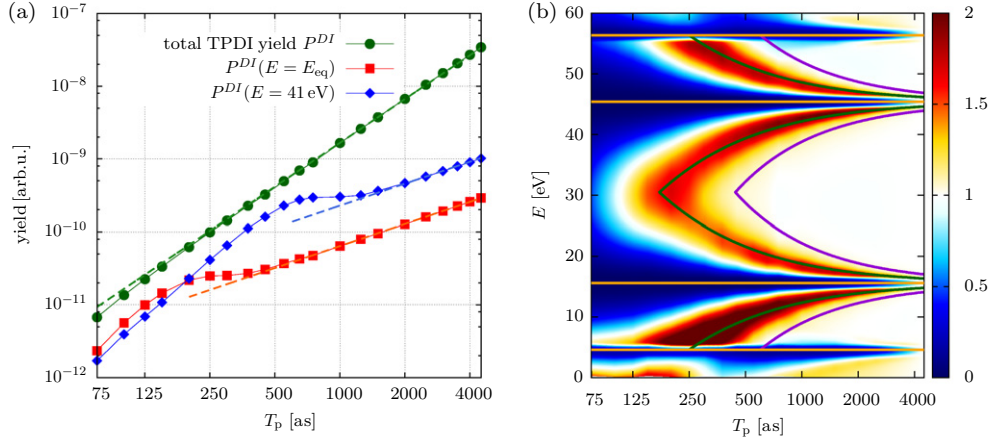**Figure 2.** (a) Scaling of two-photon double ionization yields with pulse duration T_p at $\hbar\omega = 70\,\text{eV}$. The green points are the total ionization yield P^{DI}, the red squares give the differential yield at equal energy sharing $P^{DI}(E = E_{eq})$, with $E_{eq} = (2\hbar\omega + E_0)/2$, and the blue diamonds give the differential yield at $E = 41\,\text{eV}$. The dashed lines show fits to quadratic and linear scaling with T_p for the total and singly differential yield. (b) Contour plot of $P^{DI}_{rel}(E, T_p)$. A value of 1 for P^{DI}_{rel} (white in the colour scale used here) marks the region where linear scaling of the singly differential yield with pulse duration T_p is observed. The orange lines indicate the positions of the peaks from the sequential process. The violet and green lines indicate the pulse durations $T_c^{(i)}$ and $T_c^{(ii)}$ after which linear scaling of the yield with T_p is expected due to Fourier broadening of the sequential peak and because of the maximum time delay between the photon absorptions (see the text).

energy E shows linear scaling with pulse duration. We note that the estimate of effect (ii) could be validated in a time-independent perturbation theory calculation. The latter does not show Fourier broadening but introduces an effective cutoff for the interaction time $t_c^{(ii)}$ because of the limited box size.

For long enough pulses, there is an additional interesting feature at energies $E_1 = \hbar\omega - I_1 - \mathcal{E}_2$ and $E_2 = \hbar\omega - I_2 + \mathcal{E}_2$ (see figure 1), with $\mathcal{E}_n = 2 - 2/n^2$ the excitation energy to the nth excited state in He^+. At these energies, sequential ionization via the excited ionic (shake-up) state $|nl\rangle$ is allowed. We discuss this is in more detail in section 5.

The non-uniform scaling with T_p described here should occur for any photon energy where the sequential process is allowed. This is confirmed by calculations at $\hbar\omega = 91\,\text{eV}$, shown in figure 6. At these higher photon energies, the ionized electrons obtain higher momenta, such that larger box sizes are required in the simulation for the same pulse duration. Therefore, the maximum duration of the laser pulse was restricted to $T_p = 1.5\,\text{fs}$.

4. Angular correlations

Additional information on the dynamics of the two ionized electrons can be extracted from the angular correlations in the TPDI process. To that end, we introduce the forward–backward asymmetry distribution $\mathcal{A}(E_1, E_2)$, obtained by fixing the ejection direction of one electron in the direction of the laser polarization ($\theta_1 = 0°$) and calculating the probability for the second electron to be emitted into the forward half-space $\theta_2 < \pi/2$ or backward half-space $\theta_2 > \pi/2$. The probabilities thus defined are

$$P^\pm(E_1, E_2)$$
$$= 4\pi^2 \int_{\substack{\theta_2 < \pi/2 \\ \theta_2 > \pi/2}} P(E_1, E_2, \theta_1 = 0°, \theta_2) \sin\theta_2 \, d\theta_2, \qquad (4)$$

where the factor $4\pi^2$ stems from integration over ϕ_1 and ϕ_2. The forward–backward asymmetry is then given by

$$\mathcal{A}(E_1, E_2) = \frac{P^+(E_1, E_2) - P^-(E_1, E_2)}{P^+(E_1, E_2) + P^-(E_1, E_2)}, \qquad (5)$$

which varies in the range $[-1, 1]$. Values close to zero indicate vanishing correlation between the electrons, while large absolute values identify strong angular correlations. Positive values ($\mathcal{A} > 0$) indicate a preference for ejection of both electrons in the same direction while negative values ($\mathcal{A} < 0$) indicate ejection in opposite directions. Note that $\mathcal{A}(E_1, E_2)$ is not symmetric under exchange of E_1 and E_2, as the emission direction of the electron with energy E_1 is fixed in the laser polarization direction. Analogously, the reduced one-electron asymmetry $\mathcal{A}(E_1)$ can be determined by integrating $P^\pm(E_1, E_2)$ over the energy of the second electron, i.e., $P^\pm(E_1) = \int P^\pm(E_1, E_2) \, dE_2$ and

$$\mathcal{A}(E_1) = \frac{(P^+(E_1) - P^-(E_1))}{(P^+(E_1) + P^-(E_1))}.$$

Figure 3 shows the asymmetry of TPDI at $\hbar\omega = 70\,\text{eV}$ photon energy for pulses of different duration T_p, from $T_p = 75\,\text{as}$ up to $T_p = 4500\,\text{as}$. For the shortest pulses, the electrons are dominantly ejected in opposite directions independent of energy, as observed previously [11]. As the duration is increased, a stable pattern emerges: at the 'sequential' peaks, the electrons are essentially uncorrelated, leading to vanishing asymmetry. As most electrons are ejected in this channel, the total (energy-integrated) asymmetry is very small for long pulses. However, for energies in between the two main peaks at $E_1 = \hbar\omega - I_1$ and $E_2 = \hbar\omega - I_2$, the electrons are emitted in opposite directions. This is precisely because these final state energies are reached only when the two electrons are ejected in such a configuration. This back-to-back Wannier-like emission near equal energy sharing remains pronounced even for long pulses.
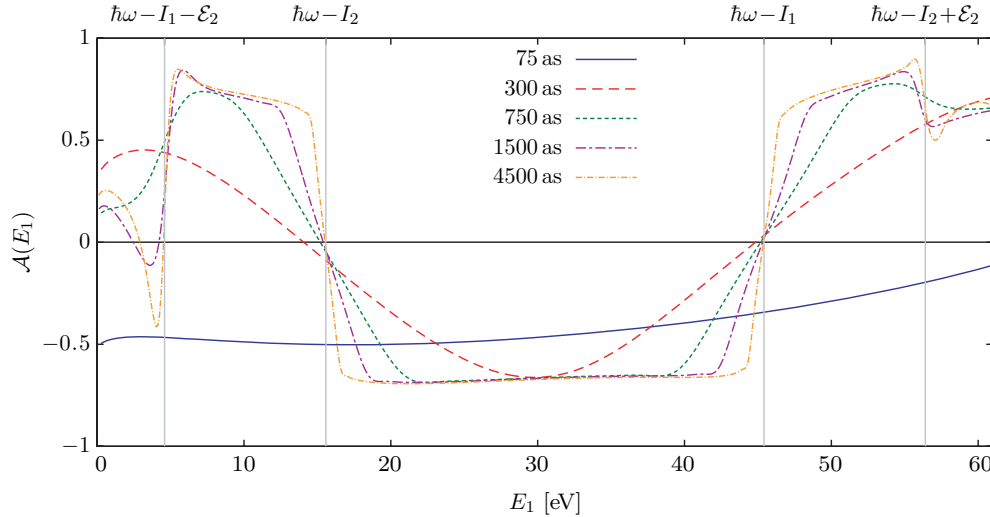
Figure 3. Forward–backward asymmetry $\mathcal{A}(E_1)$ for TPDI by an XUV pulse at $\hbar\omega = 70$ eV, for different pulse durations T_p. The grey lines show the expected positions of the peaks for the sequential process (with and without shake-up).
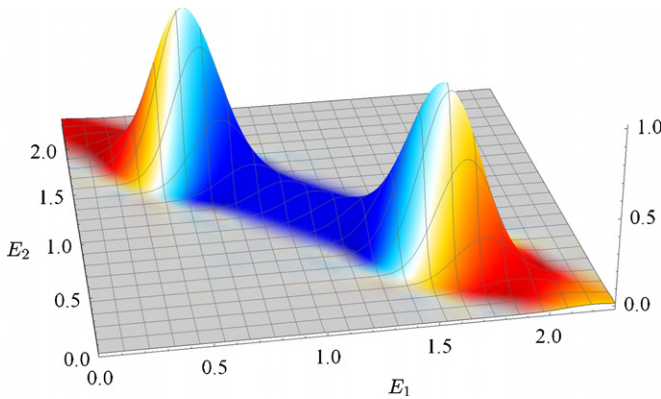

Figure 4. Combined double ionization probability $P^{DI}(E_1, E_2)$ and forward–backward asymmetry $\mathcal{A}(E_1, E_2)$ after TPDI by an XUV pulse at $\hbar\omega = 70$ eV with a duration of 450 as. The z-axis gives $P^{DI}(E_1, E_2)$ (in arbitrary units), while the colour encodes the asymmetry, with cyan to blue signifying negative values (ejection in opposite directions) and yellow to red signifying positive values (ejection in the same direction). Vanishing $\mathcal{A}$ corresponds to white. For energies where $P^{DI}(E_1, E_2)$ is negligible, the colour is set to grey.

For energies outside the energy interval delimited by the sequential peaks, the asymmetry is equally strong, but now positive, pointing to the same emission direction for both electrons. When the second electron is emitted in the same direction as the first one, the well-known post-collision interaction [50–53] tends to increase the asymmetric sharing of the available energy [11]. The dividing line between the two different regimes of ejection (in the opposite or in the same direction) is quite sharp and lies directly at the position of the sequential peaks. A more complete representation of the two-electron energy and angular correlations is presented in figure 4 for a pulse duration of $T_p = 450$ as. While the height gives the joint probability $P^{DI}(E_1, E_2)$, the colour represents the asymmetry distribution $\mathcal{A}(E_1, E_2)$. The borderline between positive and negative $\mathcal{A}$ (i.e., $\mathcal{A} = 0$, white) is precisely near the peaks associated with the sequential

process. In the central region in between the 'sequential' peaks the emission is preferentially on opposite sides while emission into the same hemisphere prevails outside the main peaks. For completeness we note that in the region between the two main peaks, only electrons emitted in opposite directions are observed both in 'sequential' ($\hbar\omega > 54.4$ eV) and 'nonsequential' (39.5 eV $< \hbar\omega < 54.4$ eV) TPDI [30]. The main difference is that in nonsequential TPDI, only that region is energetically accessible, such that no other angular configurations are observed.

5. Shake-up interferences

We return now to the additional structures at higher ($E \approx \hbar\omega - I_2 + \mathcal{E}_2$) and lower ($E \approx \hbar\omega - I_1 - \mathcal{E}_2$) energies visible in figures 1 and 3. They correspond to shake-up satellites in He$^+$ which can serve as intermediate states in sequential TPDI. In the shake-up process, the He$^+$ ion is left in an excited state, while the free electron obtains an energy of $E'_1 = \hbar\omega - I_1 - \mathcal{E}_n$ (with $\mathcal{E}_n$ the excitation energy to the nth shell of He$^+$). In the long-pulse limit, this simply leads to the appearance of shake-up satellite lines at energies E'_1 and $E'_2 = \hbar\omega - I_2 + \mathcal{E}_n$ in the one-electron energy spectrum. For ultrashort pulses, however, the nonsequential (or direct) double ionization channel becomes available as well and can lead to the same final states. Post-collision interactions lead to a broad distribution of electron energies (see section 4), so that the electrons can obtain the same final energies of $E_1^{PCI} = E'_2$ and $E_2^{PCI} = E'_1$ as the electrons emitted via He$^+(nl)$ in the sequential process. Both indistinguishable pathways lead to the same final state and thus to an interference pattern in the double ionization yield, as observed in figures 1 and 3. This interference bears some resemblance to the well-known exchange interference between, e.g. photoelectrons and Auger electrons [54–57]. There is, however, a fundamental difference: while the exchange interference is intrinsically controlled by atomic parameters, namely the
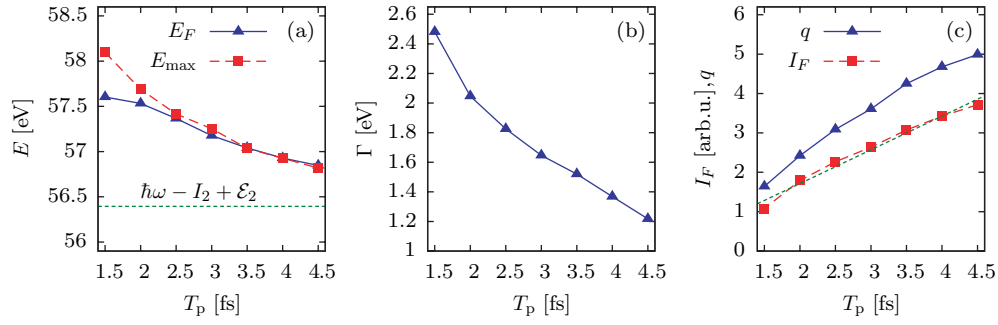
5

Figure 5. Parameters of the shake-up interference peaks around 57 eV for TPDI by an XUV pulse at $\hbar\omega = 70$ eV obtained from fitting to a Fano lineshape. (a) Fano resonance energy E_F and position $E_{\max}$ of the maximum in the spectrum, (b) width Γ, (c) Fano parameter q and integrated yield I_F from the shake-up pathway. See the text for details.

energy and lifetime (width) of the Auger electron, the novel interference observed here is truly a dynamical effect present only for short pulses and can be controlled by the pulse duration T_p.

As the dependence of the yield on the pulse duration is different for the different channels (proportional to T_p for the nonsequential channel, proportional to T_p^2 in the sequential channel), the observed spectrum strongly changes with pulse duration. For short pulses ($T_p < 500$ as, cf figure 1), the yield is completely dominated by the nonsequential channel without any trace of a shake-up interference. As the pulse duration is increased, the sequential channel with shake-up becomes increasingly important. As expected from the interference of a relatively sharp peak with a smooth background, the peak resembles a Fano lineshape [58]. Thus, the position of the maximum is shifted from the position expected in the limit of infinitely long pulses. Even for relatively long pulses ($T_p = 4.5$ fs), similar to those produced in x-ray free-electron lasers, the position of the shake-up peak in the one-electron energy spectrum $P^{DI}(E)$ is shifted by a considerable fraction of an eV. The structural similarity to a Fano resonance (a quasi-discrete resonance due to the shake-up intermediate state embedded in a smooth continuum due to the direct double ionization) suggests to characterize the interference in terms of Fano resonance parameters for the position $E_F(T_p)$, width $\Gamma(T_p)$ and asymmetry $q(T_p)$, as well as its strength $I_F(T_p)$ (figure 5). To apply Fano's parametrization [58], the calculated energy spectrum $P^{DI}(E)$ is divided by the nonresonant spectrum $P^{DI}_{\mathrm{nonres}}(E)$, taken to be proportional to the singly differential cross section as predicted from the model by Horner *et al* [39, equation (8)]. Away from the peaks, this fits the form of the spectrum very well. A background contribution c_{bg} is added to account for the different angular distributions of the different channels, which prevent complete interference. This gives

$$\frac{P^{DI}(E)}{P^{DI}_{\mathrm{nonres}}(E)} \approx c_{bg} + c_F \frac{(q\,\Gamma/2 + E - E_F)^2}{(E - E_F)^2 + (\Gamma/2)^2}. \quad (6)$$

The simple fitting procedure used here only works well for pulse durations $T_p \geqslant 1.5$ fs, as for shorter pulses, the employed approximation for the 'nonresonant' background breaks down, and the shake-up peak itself is less strong and considerably broadened. Figure 5 illustrates the dependence

of the obtained parameters on the pulse duration, confirming the expected behaviour: for long pulses, the peaks converge to the satellite lines, i.e., Lorentzians of vanishing width, such that $E_F \rightarrow \hbar\omega - I_2 + \mathcal{E}_n$ ($E_F \rightarrow \hbar\omega - I_1 - \mathcal{E}_n$), $\Gamma \rightarrow 0$, $|q| \gg 1$. The overall strength I_F of the shake-up peak relative to the nonresonant background is obtained from the integral over the Fano lineshape, $I_F \propto c_F(q^2 - 1)\Gamma$. This behaves approximately linear with T_p, confirming the scaling of the sequential shake-up channel with T_p^2 versus the scaling of the nonresonant background with T_p (figure 5(c)). Also shown in figure 5(a) is the position $E_{\max}$ of the maximum of the spectrum $P^{DI}(E)$ without any further processing.

Such effects could possibly be observed in XFEL pulses, which reach focused intensities of up to 10^{16} W cm^{-2}. To confirm that the results shown here (calculated for 10^{12} W cm^{-2}) also apply for these high intensities, we performed an additional calculation at a peak intensity of $I_0 = 5 \times 10^{15}$ W cm^{-2} with a pulse duration of $T_p = 4.5$ fs. The shape of the differential yield $P^{DI}(E)$ (not shown) is almost unchanged compared to the result at 10^{12} W cm^{-2} peak intensity, even though the ground state survival probability is only 20%. The total double ionization probability is $P^{DI} = 36\%$, i.e., more than a third of the helium atoms in the laser focus are doubly ionized. Even though the yield in the shake-up peak is only 0.6% of the total yield for that duration, this could be seen in experiment as only the integrated one-electron energy spectrum has to be observed. Moreover, from the position, strength and asymmetry of the interference peaks, information on the poorly known pulse duration of XFEL pulse 'bursts' could possibly be deduced.

The results shown up to now were obtained at a photon energy of $\hbar\omega = 70$ eV, where only the $n = 2$ shake-up channel plays a role. While the qualitative behaviour of each shake-up peak is expected to be independent of $\hbar\omega$, new intermediate ionic states $|nl\rangle$ become accessible at $\hbar\omega > I_1 + \mathcal{E}_n$, converging to $\hbar\omega > -E_0$ for $n \rightarrow \infty$ (where $E_0 \approx -79$ eV is the ground state energy of helium). This is demonstrated in figure 6 at a photon energy of $\hbar\omega = 91$ eV. As the shake-up probability strongly decreases with increasing n, only the peaks associated with $n = 2$ and $n = 3$ can clearly be identified at the pulse lengths used here (up to $T_p = 1.5$ fs). For longer pulses, more highly excited states would start to play a role as well. In that case, one would need to take into account that the
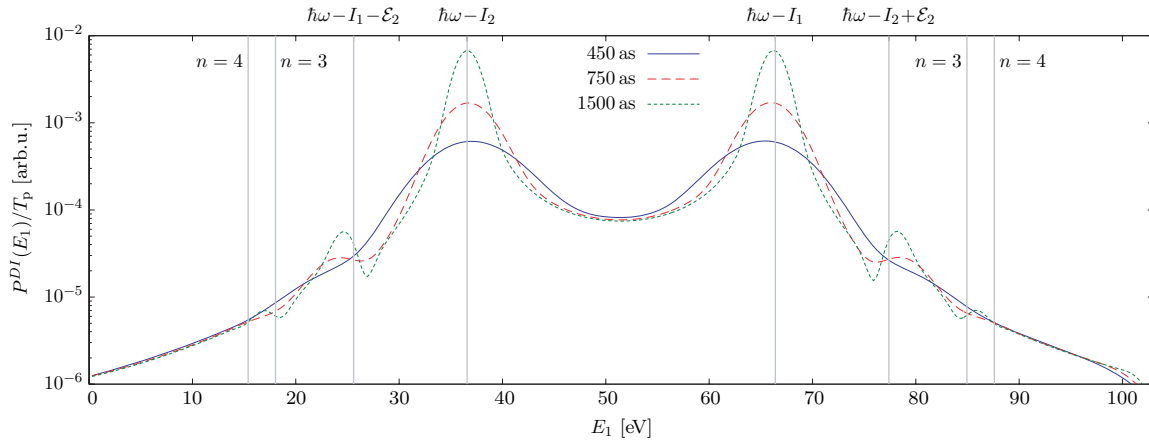
Figure 6. Double ionization (DI) rate $P^{DI}(E)/T_{\mathrm{p}}$ (i.e., DI probability divided by the pulse duration) for TPDI by an XUV pulse at $\hbar\omega = 91$ eV with different pulse durations T_{p}. Shake-up peaks up to $n = 3$ are visible.

peaks for higher n overlap with each other as well as with the nonresonant background.

It should be noted that in order to observe these interference effects, the asymptotic vectorial momenta $\mathbf{k}_1$, $\mathbf{k}_2$ (i.e., not only the asymptotic energies E_1, E_2) of the two pathways have to coincide. The shake-up channel has an angular distribution considerably different from that of the nonsequential channel, such that only partial interference between the final states is expected. This leads to a rich structure in the observed angular distributions (not shown), a more detailed analysis of which is in progress. During the preparation of this contribution, we became aware of work by Palacios *et al* [59] who also observe the interference between these different channels.

6. Summary

We have presented a detailed study of the dynamics of the two-photon double ionization process in helium in the so-called 'sequential' energy regime for a wide range of ultrashort pulse durations (75 as to 4.5 fs). We have shown how electron interaction, and thereby correlation, enforced by the short pulse duration influences the observed energy spectra and angular distributions.

The one-electron ionization rate $P^{DI}(E)/T_{\mathrm{p}}$ converges to a stable value with increasing pulse duration for energies away from the sequential peaks ($E = \hbar\omega - I_1$ and $E = \hbar\omega - I_2$), giving rise to a well-defined (direct) differential double ionization cross section. However, near the peaks where the sequential process is allowed, $P^{DI}(E)/T_{\mathrm{p}}$ grows with T_{p}. We have thus observed a non-uniform scaling of the double ionization probability with T_{p}. Even though in this spectral range the sequential process is allowed, both the direct and sequential co-exist, giving rise to interferences which are induced by the short time correlation between the two emission events. The nonsequential channel without shake-up and the sequential shake-up channel, where the intermediate state after one-photon absorption is an excited state of the He$^+$ ion, can interfere. In attosecond pulses, only the nonsequential channel contributes, while in long pulses (longer than the 4.5 fs used

here), the sequential shake-up channel dominates. For pulse durations of a few femtoseconds, as obtained in x-ray free-electron lasers, the two channels are similarly important, such that interference can be clearly observed. This interferences may open up the possibility of measuring the duration of ultrashort XUV pulses in the femtosecond regime.

We have also found that the angular distributions in the final states populated by nonsequential processes are strongly correlated. In ultrashort pulses, where the TPDI process is necessarily nonsequential, the favoured emission channel is the Wannier ridge riding mode of back-to-back emission at equal energies (cf [11]). In longer pulses, back-to-back emission is strongly favoured in the region close to equal energy sharing, while for strongly asymmetric energy sharing, the electrons are primarily emitted in the same direction.

References

[1] Hentschel M, Kienberger R, Spielmann C, Reider G A, Milosevic N, Brabec T, Corkum P, Heinzmann U, Drescher M and Krausz F 2001 *Nature* **414** 509
[2] Sansone G *et al* 2006 *Science* **314** 443
[3] Goulielmakis E *et al* 2008 *Science* **320** 1614
[4] Ackermann W *et al* 2007 *Nat. Photonics* **1** 336
[5] Nabekawa Y, Hasegawa H, Takahashi E J and Midorikawa K 2005 *Phys. Rev. Lett.* **94** 043001
[6] Dromey B *et al* 2006 *Nat. Phys.* **2** 456

[7] Naumova N M, Nees J A, Sokolov I V, Hou B and Mourou G A 2004 *Phys. Rev. Lett.* **92** 063902

[8] Seres J, Yakovlev V S, Seres E, Streli C, Wobrauschek P, Spielmann C and Krausz F 2007 *Nat. Phys.* **3** 878

[9] Zhang X, Lytle A L, Popmintchev T, Zhou X, Kapteyn H C, Murnane M M and Cohen O 2007 *Nat. Phys.* **3** 270

[10] Nomura Y *et al* 2009 *Nat. Phys.* **5** 124

[11] Feist J, Nagele S, Pazourek R, Persson E, Schneider B I, Collins L A and Burgdörfer J 2008 arXiv:0812.0373

[12] Parker J S, Smyth E S and Taylor K T 1998 *J. Phys. B: At. Mol. Opt. Phys.* **31** L571

[13] Byron F W and Joachain C J 1967 *Phys. Rev.* **164** 1

[14] Proulx D and Shakeshaft R 1993 *Phys. Rev.* A **48** R875

[15] Bräuning H *et al* 1998 *J. Phys. B: At. Mol. Opt. Phys.* **31** 5149

[16] Briggs J S and Schmidt V 2000 *J. Phys. B: At. Mol. Opt. Phys.* **33** R1

[17] Malegat L, Selles P and Kazansky A K 2000 *Phys. Rev. Lett.* **85** 4450

[18] Lein M, Gross E K U and Engel V 2000 *Phys. Rev. Lett.* **85** 4707

[19] Staudte A *et al* 2007 *Phys. Rev. Lett.* **99** 263002

[20] Rudenko A, de Jesus V L B, Ergler T, Zrost K, Feuerstein B, Schröter C D, Moshammer R and Ullrich J 2007 *Phys. Rev. Lett.* **99** 263003

[21] Nikolopoulos L A A and Lambropoulos P 2001 *J. Phys. B: At. Mol. Opt. Phys.* **34** 545

[22] Colgan J and Pindzola M S 2002 *Phys. Rev. Lett.* **88** 173002

[23] Feng L and van der Hart H W 2003 *J. Phys. B: At. Mol. Opt. Phys.* **36** L1

[24] Hu S X, Colgan J and Collins L A 2005 *J. Phys. B: At. Mol. Opt. Phys.* **38** L35

[25] Foumouo E, Lagmago Kamta G, Edah G and Piraux B 2006 *Phys. Rev.* A **74** 063409

[26] Ivanov I A and Kheifets A S 2007 *Phys. Rev.* A **75** 033411

[27] Nikolopoulos L A A and Lambropoulos P 2007 *J. Phys. B: At. Mol. Opt. Phys.* **40** 1347

[28] Pronin E A, Manakov N L, Marmo S I and Starace A F 2007 *J. Phys. B: At. Mol. Opt. Phys.* **40** 3115

[29] Horner D A, McCurdy C W and Rescigno T N 2008 *Phys. Rev.* A **78** 043416

[30] Feist J, Nagele S, Pazourek R, Persson E, Schneider B I, Collins L A and Burgdörfer J 2008 *Phys. Rev.* A **77** 043420

[31] Antoine P, Foumouo E, Piraux B, Shimizu T, Hasegawa H, Nabekawa Y and Midorikawa K 2008 *Phys. Rev.* A **78** 023415

[32] Guan X, Bartschat K and Schneider B I 2008 *Phys. Rev.* A **77** 043421

[33] Hasegawa H, Takahashi E J, Nabekawa Y, Ishikawa K L and Midorikawa K 2005 *Phys. Rev.* A **71** 023407

[34] Sorokin A A, Wellhofer M, Bobashev S V, Tiedtke K and Richter M 2007 *Phys. Rev.* A **75** 051402

[35] Laulan S and Bachau H 2003 *Phys. Rev.* A **68** 013409

[36] Piraux B, Bauer J, Laulan S and Bachau H 2003 *Eur. Phys. J.* D **26** 7

[37] Ishikawa K L and Midorikawa K 2005 *Phys. Rev.* A **72** 013407

[38] Barna I F, Wang J and Burgdörfer J 2006 *Phys. Rev.* A **73** 023402

[39] Horner D A, Morales F, Rescigno T N, Martín F and McCurdy C W 2007 *Phys. Rev.* A **76** 030701

[40] Foumouo E, Antoine P, Bachau H and Piraux B 2008 *New J. Phys.* **10** 025017

[41] Ullrich J, Moshammer R, Dorn A, Dörner R, Schmidt L P H and Schmidt-Böcking H 2003 *Rep. Prog. Phys.* **66** 1463

[42] Pindzola M S *et al* 2007 *J. Phys. B: At. Mol. Opt. Phys.* **40** R39

[43] Rescigno T N and McCurdy C W 2000 *Phys. Rev.* A **62** 032706

[44] McCurdy C W, Horner D A and Rescigno T N 2001 *Phys. Rev.* A **63** 022711

[45] Schneider B I and Collins L A 2005 *J. Non-Cryst. Solids* **351** 1551

[46] Schneider B I, Collins L A and Hu S X 2006 *Phys. Rev.* E **73** 036708

[47] Park T J and Light J C 1986 *J. Chem. Phys.* **85** 5870

[48] Smyth E S, Parker J S and Taylor K T 1998 *Comput. Phys. Commun.* **114** 1

[49] Leforestier C *et al* 1991 *J. Comp. Phys.* **94** 59

[50] Barker R B and Berry H W 1966 *Phys. Rev.* **151** 14

[51] Gerber G, Morgenstern R and Niehaus A 1972 *J. Phys. B: At. Mol. Phys.* **5** 1396

[52] Russek A and Mehlhorn W 1986 *J. Phys. B: At. Mol. Phys.* **19** 911

[53] Armen G B, Tulkki J, Åberg T and Crasemann B 1987 *Phys. Rev.* A **36** 5606

[54] Végh L and Macek J H 1994 *Phys. Rev.* A **50** 4031

[55] Read F H 1977 *J. Phys. B: At. Mol. Phys.* **10** L207

[56] de Gouw J A, van Eck J, Peters A C, van der Weg J and Heideman H G M 1993 *Phys. Rev. Lett.* **71** 2875

[57] Rouvellou B, Rioual S, Avaldi L, Camilloni R, Stefani G and Turri G 2003 *Phys. Rev.* A **67** 012706

[58] Fano U 1961 *Phys. Rev.* **124** 1866

[59] Palacios A, Rescigno T N and McCurdy C W 2009 *Phys. Rev.* A **79** 033402